Biophysical Journal
Article

Biophysical Society

Toxic HypF-N Oligomers Selectively Bind the Plasma Membrane to Impair Cell Adhesion Capability

Reinier Oropesa-Nuñez,[1,2] Sandeep Keshavan,[1,2] Silvia Dante,[1] Alberto Diaspro,[1,3,*] Benedetta Mannini,[4] Claudia Capitini,[5] Cristina Cecchi,[5] Massimo Stefani,[5] Fabrizio Chiti,[5] and Claudio Canale[1,3]

[1]Department of Nanophysics, Istituto Italiano di Tecnologia, Genova, Italy; [2]DIBRIS Department, University of Genova, Genova, Italy; [3]Department of Physics, University of Genova, Genova, Italy; [4]Department of Chemistry, University of Cambridge, Cambridge, United Kingdom; and [5]Section of Biochemistry, Department of Experimental and Clinical Biomedical Sciences, University of Florence, Firenze, Italy

ABSTRACT The deposition of fibrillar protein aggregates in human organs is the hallmark of several pathological states, including highly debilitating neurodegenerative disorders and systemic amyloidoses. It is widely accepted that small oligomers arising as intermediates in the aggregation process, released by fibrils, or growing in secondary nucleation steps are the cytotoxic entities in protein-misfolding diseases, notably neurodegenerative conditions. Increasing evidence indicates that cytotoxicity is triggered by the interaction between nanosized protein aggregates and cell membranes, even though little information on the molecular details of such interaction is presently available. In this work, we propose what is, to our knowledge, a new approach, based on the use of single-cell force spectroscopy applied to multifunctional substrates, to study the interaction between protein oligomers, cell membranes, and/or the extracellular matrix. We compared the interaction of single Chinese hamster ovary cells with two types of oligomers (toxic and nontoxic) grown from the N-terminal domain of the *Escherichia coli* protein HypF. We were able to quantify the affinity between both oligomer type and the cell membrane by measuring the mechanical work needed to detach the cells from the aggregates, and we could discriminate the contributions of the membrane lipid and protein fractions to such affinity. The fundamental role of the ganglioside GM1 in the membrane-oligomers interaction was also highlighted. Finally, we observed that the binding of toxic oligomers to the cell membrane significantly affects the functionality of adhesion molecules such as Arg-Gly-Asp binding integrins, and that this effect requires the presence of the negatively charged sialic acid moiety of GM1.

INTRODUCTION

The self-assembly of peptide/protein molecules from their native states into well-defined fibrillar aggregates in human tissues is associated with a number of degenerative pathologies, including Alzheimer's, Parkinson's, Huntington's diseases, several systemic amyloidoses, and many others (1). In many such diseases, particularly in neurodegenerative conditions, it is currently believed that an important cytotoxic role is played by small protein oligomers that accumulate as on- or off-pathway species during fibril formation (2–5), can be released by leakage from mature amyloid fibrils (2,6–8), or can result as a consequence of secondary nucleation at the surface of preformed fibrils (9–12).

The two oligomeric forms, named type A oligomer (OA) and type B oligomer (OB) and grown under different solution conditions from the N-terminal domain of the *Escherichia coli* protein HypF (HypF-N), have provided a remarkable contribution to our understanding of the oligomer structure-cytotoxicity relationship (13–20). In particular, this system has allowed us to gain significant insight into the structural and biophysical determinants underlying the interaction of protein-misfolded oligomers with the cell membrane, in most cases the earliest event in oligomer-mediated cytotoxicity (13–20). Both OAs and OBs bind weakly, but significantly, to thioflavin T and display a roughly spherical shape with a height of 2–6 nm as determined by atomic force microscopy (AFM) (13). However, only OAs were found to be cytotoxic when added to the extracellular medium of cultured cells (13–15,17,20) or injected into rat brain (19,20), similarly to oligomers found in other amyloid diseases (21). It is just the toxic and nontoxic

Submitted August 31, 2017, and accepted for publication February 2, 2018.

*Correspondence: alberto.diaspro@iit.it

Editor: Joseph Zasadzinski.

https://doi.org/10.1016/j.bpj.2018.02.003

natures of OAs and OBs, respectively, that through a comparative study of the two forms have provided an important contribution to the elucidation of the oligomer structural determinants underlying their toxicity and eventually culminating with cell dysfunction and death (13–20,22).

Previous experimental evidence suggested that the different toxicities of OA and OB are attributable to the higher solvent-exposure of hydrophobic amino acid residues in the former with respect to the latter (13). At micromolar concentrations, both OA and OB interact with the cell membrane of cultured cells, but only OAs destabilize the membrane, causing several biochemical modifications that eventually lead to cell failure (20). Subsequent studies showed that the interaction of OAs with the cell membrane occurs at lipid rafts (membrane lipid domains enriched in cholesterol, sphingolipids, and the GM1 ganglioside), and that such interaction is mediated particularly by the latter (14,15,18). The use of different forms of oligomers of the Aβ_{42} peptide (named A+ and A− (23)) with different structural properties and cytotoxicity yielded comparable results, further highlighting the importance of solvent-exposed hydrophobic clusters as well as oligomer-membrane interaction and lipid composition, particularly GM1 content, in determining protein-oligomer cytotoxicity (14,15,24–26). More generally, GM1 has been repeatedly shown to be involved in amyloid fibril growth and recruitment of amyloidogenic proteins to the cell membrane, supporting its remarkable role in amyloid growth and cytotoxicity not only in vitro but also in vivo (27–31). Moreover, the similarity of the results obtained with the two types of HypF-N and Aβ_{42} oligomers supports the validity of using the former to carry out further studies on the relationship between membrane lipid composition/GM1 content on the one hand and oligomer structure/physicochemical properties/toxicity on the other.

A recent detailed study carried out by AFM imaging on supported lipid bilayers (SLBs) has elucidated the different ability of the two types of oligomers to interact with the GM1-enriched gel phase domains (Lβ domains) and/or the fluid domains (Lα domains) of the bilayer (18). Interestingly, OAs, but not OBs, were able to interact with both Lα and Lβ domains. In particular, OAs were found to penetrate the ordered Lβ domains of the SLBs, whereas they assembled into annular species in the fluid Lα domains. The same study revealed that the cleavage and elimination of the sialic acid group from GM1 in the Lβ domains of SLBs and in the lipid membrane rafts of cultured cells inhibited both the interaction of the OAs with the Lβ domains of the SLBs and their cytotoxicity (18). This finding indicated that only the interaction of OA with the Lβ phase domains is responsible for cytotoxicity, and that this interaction is driven by electrostatic attraction between the negatively charged GM1 and the positively charged Hypf-N (32). It also provided clues against the theory based on oligomer cytotoxicity through formation of annular doughnut-shaped oligomers in the cell membrane, in agreement with recent data (33–36).

Oligomer toxicity has also been proposed to depend on the interaction not only with the lipid fraction of the cell membrane but also with membrane proteins most often located within the lipid rafts (37). Preliminary data have reported that both OAs and OBs interact with cell membrane proteins, and that nontoxic OBs are stronger binders of proteins (unpublished data). Overall, both toxic OAs and nontoxic OBs have been reported to interact with membrane protein components, but only OAs appear to interact with the lipid components of the cell membrane, and such interaction, particularly when mediated by GM1 in the ordered-phase domains of SLBs or in the lipid rafts of the cell membrane, appears to be responsible for OA-mediated toxicity.

Early on, the scanning probe microscopy community recognized the potential of AFM for measuring bond strengths. Indeed, AFM has been widely used in the study of intermolecular interactions, i.e., well-defined chemical functionalities, protein-protein pairs, and colloidal particles (38–43). The coupling with fluorescent optical microscopy has been the most common solution exploited to overcome the lack of chemical specificity of AFM (44–46). In this work, we exploited a method based on single-cell force spectroscopy (SCFS) (47–54) and previously described by our group to investigate the adhesion of single cells on multifunctional substrates (52) to study quantitatively the mechanical forces associated with the interaction between cell membranes and protein oligomers, which is a yet unexplored field. In particular, we characterized in more detail the interaction force between toxic/nontoxic oligomers and the cell membrane by using OA and OB as a model of oligomers and Chinese hamster ovary (CHO) cells as a probe. CHO cells are particularly suitable to this purpose and have been widely employed in SCFS applications (50,52,54,55). Furthermore, they have been also used as a model system to test protein aggregate toxicity (56–58), permitting a comparison of our data with those reported in the literature. The interaction between OA/OB species and the cell membrane was quantified as the mechanical work needed to detach a number of individual protein aggregate particles from the cell membrane. This approach allowed the quantification of the relative affinities of the toxic OA oligomers for the membrane lipid and protein fractions. Our results also indicate the need of a deeper analysis on the influence of OA/OB on the functionality of classes of membrane molecules other than lipids and their interaction with extracellular matrix components.

MATERIALS AND METHODS

Preparation of HypF-N amyloid aggregates

HypF-N was purified, and its aggregated forms were obtained as previously described (13). In brief, in the first conditions, defined as conditions A, we

obtained OAs and type A fibrils (FAs), whereas in second conditions, conditions B, we obtained OBs and type B protofibrils (PFBs). In type A conditions, native HypF-N was diluted to 48 μM in 50 mM acetate buffer (pH 5.5) containing 12% (v/v) trifluoroethanol (Sigma-Aldrich, St. Louis, MO) and 2.0 mM dithiothreitol (Sigma-Aldrich) and incubated for 4 h and 21 days at 25°C, respectively. In the type B conditions, native HypF-N was diluted to 48 μM in 20 mM trifluoroacetic acid (Sigma-Aldrich), and 330 mM NaCl (pH 1.7), followed by incubation at 25°C for 4 h and 21 days, respectively. The samples were then centrifuged at 16,100 $\times$ g for 10 min and resuspended in 10.0 mM Na_2HPO_4, 2.7 mM KCl, 137 mM NaCl (pH 7.4) (PBS; Sigma-Aldrich), or in cell culture medium, at a final protein concentration of 0.5 mg/mL (48 μM).

CHO cell culture

CHO cells (CCL-61T; ATCC, Teddington, United Kingdom) were cultured on petri dishes (Techno Plastic Products, Neuchâtel, Switzerland) coated with poly-D-lysine (PDL; Sigma-Aldrich), in Dulbecco's modified Eagle's medium (Gibco, Paisley, United Kingdom) containing 4.5% glutamine and glucose, 10% inactivated fetal bovine serum, 1.0% penicillin-streptomycin, and 1.0% nonessential amino acids (Gibco) at 37°C in 5.0% CO_2. The cells were split every 4–5 days before reaching confluency. In a set of experiments, CHO cells were treated with a neuraminidase (NAA) cocktail to remove the sialic acid group from GM1 in the plasma membrane; the cell culture medium was replaced with a new solution of the same medium containing 117 mU/mL of *Vibrio cholerae* NAA and 33 mU/mL of *Arthrobacter ureafaciens* NAA (both from Sigma-Aldrich). The cells were incubated for 60 min at 37°C with the NAA cocktail and subsequently rinsed three times with PBS before further measurements.

Preparation of functionalized surface for SCFS

Three-dimensional (3D) N-hydroxysuccinimidil (NHS) coverslips (PolyAn, Berlin, Germany) were used to anchor the molecules of interest to the glass substrate. 3D-NHS coverslips consisted of a glass substrate that was functionalized with branched polymers presenting a combination of reactive NHS-ester functional groups with PolyAn antifouling matrix (PolyAn, Berlin, Germany). The functional NHS-ester reacts with the NH_2 groups of biological species (such as lysine side chains or N-termini in proteins). The antifouling matrix prevents nonspecific attachment. This branched polymer was covalently linked to the glass substrate of the coverslip and had a typical thickness of ~50 nm.

Then 2.0 μL of samples containing 12 μM HypF-N in aggregated form (OA, OB, FA, PFB) in PBS were spotted on the 3D-NHS coverslips and incubated 15 min at room temperature in a closed chamber at 100% relative humidity. The samples were gently rinsed twice with PBS, then all free and nonreacted NHS-esters were blocked by incubating the coverslips with the blocking solution (PolyAn). At the end of the incubation, the blocking solution was discharged, and the samples were rinsed three times with PBS. The functionalized substrates were used in the same day of the preparation.

Cantilever functionalization and cell capture

Silicon tipless cantilevers TL1-50 with a nominal spring constant of 0.03 N/m (NanoWorld, Neuchâtel, Switzerland) were irradiated in an ultraviolet/ozone cleaner (ProCleaner; Bioforce Nanosciences, Ames, IA) for 15 min before functionalization to remove organic contaminations and to increase the hydrophilicity of the cantilever. The cantilevers were functionalized for cell attachment with concanavalin A (Sigma-Aldrich) as described previously (59). The actual spring constant of each cantilever was determined in situ using the thermal noise method, as described previously (60). Following a previously reported procedure (52), a 10 μL aliquot of a 0.15% w/w agarose solution (Sigma-Aldrich) was spread in a small area of the substrate until gelification, as the lack of adhesion between the cell and the repulsive agarose significantly increased the capability of the cantilever to capture a cell, as previously shown (52).

For cell attachment, CHO cells were removed from the petri dish via trypsinization: the culture medium was removed, and the cells were first incubated with 0.5% trypsin-EDTA (Gibco) for 2 min and then placed in PBS buffer and centrifuged for 5 min at 200 $\times$ g. After centrifugation, the cells were resuspended in PBS and gently agitated; a few detached cells were injected into the AFM liquid cell. A single cell was captured by pressing for 30 s the functionalized cantilever onto a cell lying on the agarose spot with a controlled force of 2.0 nN, and then by lifting the cantilever. Ten to fifteen minutes were spent waiting to get a stable cell-cantilever contact. An optical image showing a CHO cell attached to the AFM cantilever is shown in Fig. S1.

SCFS

A force-distance (F-D) curve-based AFM application, SCFS, was employed to test the interaction between a single CHO cell and the tested interactors. SCFS experiments were carried out using a Nanowizard III system (JPK Instruments, Berlin, Germany), coupled with an AxioObserver D1 (Zeiss, Oberkochen, Germany) inverted optical microscope. A CellHesion module (JPK Instruments) was used to extend to 100 μm the vertical displacement range of the AFM.

In each experiment, the cell attached to the AFM cantilever was lowered at a constant speed of 5.0 μm/s until the cell made contact with the substrate-bound protein aggregates and the preset force of 2.0 nN was reached. The contact was kept for 30 s, maintaining the force constant at 2.0 nN. Then the cell was retracted, lifting the cantilever at a constant velocity of 5.0 μm/s to register the F-D curve. The force-curve length was set at 80 μm to achieve complete detachment of the cell from the molecular substrate. The F-D curves were corrected for the bending of the cantilever (61,62) to calculate the force versus cell-sample separation curve. After removing the baseline offset because of hydrodynamic drag, the detachment work (W) was determined by integrating the force over the retraction distance (cell-sample separation) below the baseline at 0 nN of force. All the curves were processed with the JPK Data Processing software, and the data were analyzed with OriginPro 9.1 (OriginLab, Northampton, MA).

All experiments were carried out at 37°C in PBS containing 2.0 mM $CaCl_2$ and 2.0 mM $MgCl_2$. The spots of the different protein aggregates were tested sequentially with the same cell. In some cases, after the acquisition of the first set of F-D curves, the Arg-Gly-Asp (RGD) tripeptide (Sigma-Aldrich) was added at a final concentration of 200 μM to block specific integrin binding. RGD was left for 25 min before the acquisition of a second set of F-D curves on the same positions previously tested.

Cell adhesion on PDL

2.0 μL of PDL (molecular weight of 70,000; Sigma-Aldrich) dissolved in water at a concentration of 10^{-2} M was deposited on standard glass coverslips and incubated for 15 min at room temperature in a closed humid chamber (relative humidity 100%). Then the coverslips were rinsed with deionized water. F-D curves were acquired on PDL-coated substrates as described above. Then 48 μM of OA or OB solution in PBS were injected in the measurement medium to a final concentration of 12 μM and left in incubation for 25 min before the acquisition of new sets of F-D curves.

Confocal scanning microscopy

CHO cells were seeded on standard PDL-coated glass coverslips using the same procedure previously described (CHO Cell Culture) in the absence or presence of OA or OB at a final concentration of 12 μM (monomer equivalent). Similarly, CHO cells treated with the NAA cocktail for 60 min at

37°C (as previously described in CHO Cell Culture) were rinsed three times with PBS before seeding on standard PDL-coated glass coverslips in the presence of OA or OB. After seeding, the cells were fixed with 4.0% (w/v) paraformaldehyde (SC Biotechnology, Santa Cruz, CA) in PBS at different time intervals (24 and 48 h). The coverslips were washed once with prewarmed PBS and fixed using 4.0% paraformaldehyde for 10 min at room temperature. Cells were permeabilized with 0.1% Triton X-100 in PBS for 3–5 min, then 1.0% bovine serum albumin (Sigma-Aldrich) in PBS was administered to reduce nonspecific background. For selective F-actin staining, cells were incubated for 20 min at room temperature in a solution of Alexa Fluor-647 phalloidin (Life Technologies, Carlsbad, CA) diluted in PBS at a final concentration of 6.6 μM. Finally, the cells were air-dried and mounted on microscope slides by a permanent ProLong (Thermo Fisher Scientific, Boston, MA) antifade reagent with 4′, 6-diamidino-2-phenylindole. Fluorescence imaging was performed with a Nikon Inverted Microscope TiE equipped with a Nikon Confocal Laser System (Nikon Optical, Ltd., Tokyo, Japan) with excitation at 405 and 647 nm. The confocal microscope was set at optimal acquisition conditions of pinhole diameter, detector gain, and laser power, and the settings were kept constant for each analysis.

RESULTS

Toxic HypF-N oligomers interact strongly with the cell membrane

The interaction between individual CHO cells and either toxic OAs or nontoxic OBs was studied using SCFS. Cell interaction with the large FA (see Materials and Methods) and PFB (see Materials and Methods) aggregates was also investigated. OA, OB, FA, and PFB were bound to 3D-NHS coverslips. The binding to the glass substrate of the 3D-NHS coverslips was mediated by the presence of long and flexible polymeric molecules with a terminal group (NHS) that binds covalently the NH_2 groups of proteins (see Materials and Methods). Protein aggregates were spotted in confined areas of the 3D-NHS coverslip, identified by markers at the bottom side of the coverslip to be easily accessible for AFM investigation. Single CHO cells were captured on a tipless AFM cantilever (see Materials and Methods). A cartoon of a glass substrate functionalized with a HypF-N aggregate and of a CHO cell captured to the tipless AFM cantilever is shown in Fig. 1 *A*.

At the beginning of each experiment, the cell was in contact with the functionalized substrate with a defined force (Fig. 1 *B*, time point I). Then the AFM cantilever started to move away from substrate-bound aggregates, with the maximal adhesion force reached later; at this time, no adhesion interactions had been broken, but the cantilever was deflected and applied a traction force to the cell (Fig. 1 *B*, time point II). Then the cell began its progressive detachment from the substrate-bound protein aggregate through several dissociation events, generally seen in the F-D curve as a number of jumps of the traction force followed by plateaus (Fig. 1 *B*, time point III), as previously described (49). When the cell was fully detached, a final plateau at force ~0 nN was reached (Fig. 1 *B*, time point IV). This experiment yielded a F-D curve for which *W*, corresponding to the gray area below the baseline at 0 nN of force (Fig. 1 *C*), was the physical parameter used to quantify the interaction between the cell and the substrate-bound protein aggregate, representing the total energy associated with cell detachment from the aggregates.

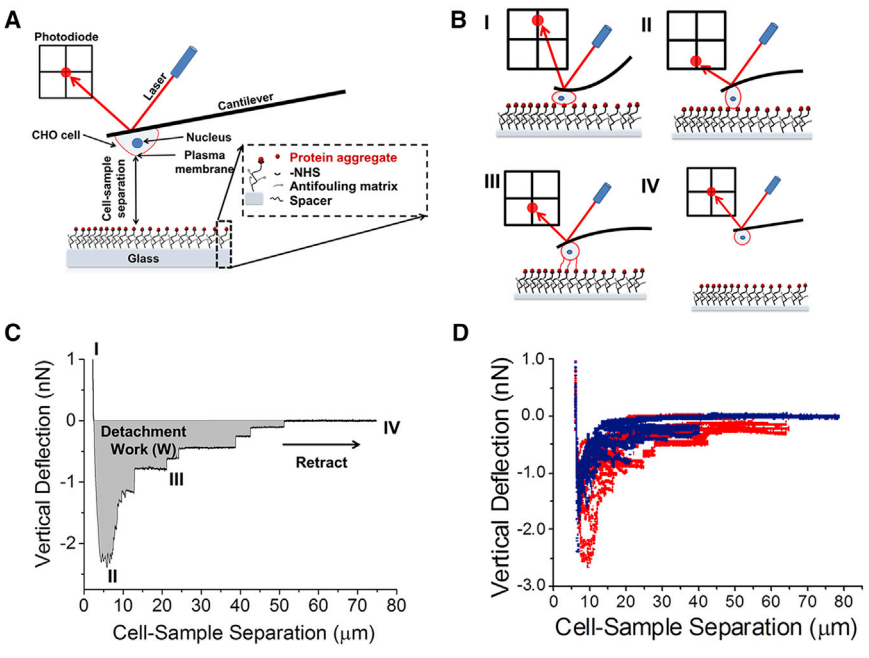

FIGURE 1 (*A*) gives a schematic description of all the components of the SCFS system. In (*B*), the four time points of the experiment are represented as a cartoon. At the beginning the cell is in contact with the functionalized substrate with a defined force (I); the AFM cantilever then starts to move away from the substrate until the maximal adhesion force has been reached; at this time no adhesion interactions have been broken, but the cantilever is deflected and is applying a traction force on the cell (II); then, the cell begins its detachment from the proteins linked to the substrate; the detachment process is characterized by several rupture events, generally defined as a number of jumps of the traction force (III) (49); finally, the cell is fully detached when a final plateau at force ~0 nN is reached (IV). (*C*) shows the typical F-D curve acquired in SCFS with the four time points described in (*B*). The detachment work (*W*) is the physical quantity monitored to quantify the interaction between the cell and the protein bound to the substrate and is represented by the gray area below the baseline at 0 nN of force. (*D*) shows two batches of F-D curves, acquired on OA (*red*) and OB (*blue*) with a single CHO cell as described in Materials and Methods. The same number of F-D curves (n = 23) was acquired for both OA and OB, and all the 46 F-D curves are plotted. F-D curves were aligned at the contact point. To see this figure in color, go online.

Over 15 F-D curves per spot (i.e., for each single protein aggregate) were acquired for every single cell; 13 single CHO cells were tested for a total of 252 F-D curves (Fig. 1 *D*). The value of *W* obtained on the bare substrates, i.e., on a portion of the 3D-NHS coverslip free of aggregates and after blocking the NHS groups, was considered as control value (here called CTR). The values of *W* obtained for the four distinct aggregate types were compared (Fig. 2).

The value of *W* determined for OA was remarkably higher ($p \leq 0.001$) than that determined for OB (Fig. 2 *B*). The *W*-values obtained for FA and PFB were both significantly lower ($p \leq 0.001$) than those obtained for OA and OB (Fig. 2 *B*). These data agree with the higher affinity to the cell membrane found previously for OA with respect to OB (13,15,18–20) and confirm the scarce interaction of PFB and mature FA aggregates with the cell membrane (63,64) (Fig. 2 *B*).

GM1 partially mediates the interaction between OA and the cell membrane

After measuring the interaction force with the cell membrane of the investigated aggregates, we sought to identify the molecules and the main chemical group(s) in the cell membrane responsible for its strong interaction with OA; in particular, considering our previous results, we focused on GM1 and its sialic acid moiety. The experiments described above were repeated on CHO cells containing membrane GM1 lacking its negatively charged sialic acid group after treatment with NAA (see Materials and Methods). Over 15 F-D curves per each spot were acquired for every single CHO cell; 13 cells were tested for a total of 245 F-D curves. In this case, the *W*-values determined for OB, PFB, and FA were not different, within experimental error, from those obtained with cells containing GM1 (Fig. 2 *B*), whereas a significant decrease ($p \leq 0.001$) of the *W*-value was obtained on OA (Fig. 2 *B*) such that the *W*-values recorded for OB and OA became similar ($p > 0.05$) (Fig. 2 *B*).

This result also reveals the contribution of membrane proteins and membrane lipids to the measured *W*-value for detaching OA from the cell membrane. Indeed, removal of the sialic group of the GM1 ganglioside, which is the main mediator of the lipid raft-OA interaction and associated toxicity (15,18), reduces to approximately one-half of the *W*-value to detach OA for the membrane. Such a residual *W*-value measured after removal of the sialic group results from the work required to detach OA from the disordered fluid phase of the membrane, which is not mediated by GM1 (18), and from the protein components of the membrane. We can therefore determine that the lipids in the GM1-containing lipid rafts contribute to approximately one-half of the overall affinity between OA and the membrane, and that the remaining half is contributed by membrane proteins and non-lipid-raft phospholipids. Considering the negligible interaction of large aggregates (FA, PFB) with the cell membrane, only the OA and OB aggregates were further investigated.

The interaction between OA/OB and cells influences cell adhesion capability

After describing the importance of GM1 as a key determinant of the force HypF-N aggregates interacting with the cell membrane, we investigated the modulation by the oligomers of cell adhesion to the substrate by testing the ability of CHO cells to adhere to PDL, a widely used adhesion factor and an extracellular matrix mimetic, before and after administration of 12 μM OA or OB (monomer concentration equivalent). This experiment is described schematically in Fig. 3 *A*. We initially tested the adhesion of a single cell to a uniformly PDL-coated substrate at different points of the surface ($n > 20$) in the absence of HypF-N oligomers by acquiring one F-D curve per position. Then the cell was allowed to interact with OA or OB for 25 min before the acquisition of a new set of F-D curves in the same positions (again, one F-D curve per position). The experiments were repeated with 12 CHO cells for each type of oligomer for a total of ~250 F-D curves acquired before and after oligomer administration to the cells. Being particularly interested in the variation of *W* upon oligomer administration, all *W*-values were normalized to those obtained with PDL before oligomer addition (W_0). After OA administration, the detachment work was remarkably reduced ($W/W_0 = 0.25 \pm 0.07$, $p \leq 0.001$) with respect to that recorded before oligomer addition (Fig. 3 *B*),

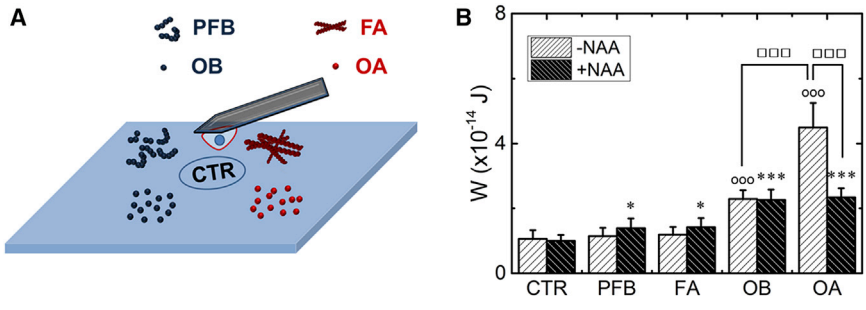

FIGURE 2 (*A*) shows a schematic representation of the distribution of OA, OB, FA, and PFB aggregates on the functionalized glass substrate. (*B*) shows the mean work spent to detach the cell from the substrate (*W*) for the various aggregate types and obtained with cells treated with and without NAA. Error bars correspond to standard deviations. * and *** indicate $p \leq 0.05$ and $p \leq 0.001$, respectively, relative to CTR. ° ° ° indicates $p \leq 0.001$ relative to CTR in the experiments on cells untreated with NAA. □□□ indicates $p \leq 0.001$ in the indicated comparisons. To see this figure in color, go online.

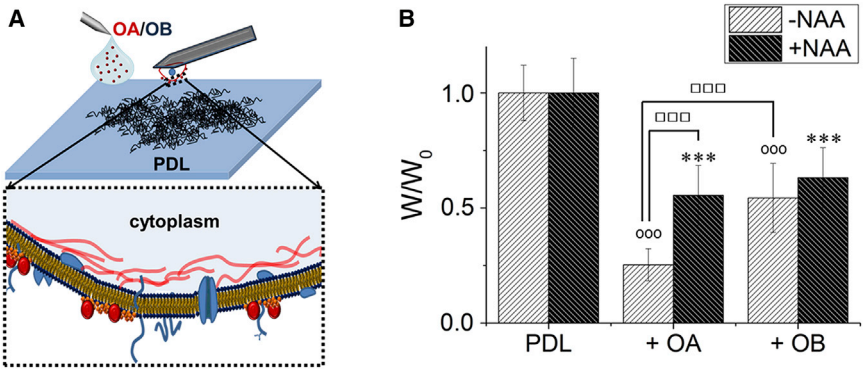

FIGURE 3 (*A*) shows a schematic representation of the SCFS experiment performed to test CHO cell adhesion on a standard adhesion molecule, i.e., PDL, in the absence and presence of OA or OB. (*B*) shows the mean work spent to detach the cell from PDL-coated substrates obtained in the absence (PDL) and in the presence of OA/OB (+OA/+OB). Results obtained on NAA treated cells are represented by the black bars. All the results are normalized to the corresponding value obtained in the absence of protein aggregate, here indicated as W_0. Error bars correspond to standard deviations. *** and $^{\circ\circ\circ}$ indicate $p \leq 0.001$ relative to PDL. $^{\square\square\square}$ indicates $p \leq 0.001$ in the indicated comparisons. To see this figure in color, go online.

whereas after OB administration, the detachment work was also significantly, yet less remarkably, decreased ($W/W_0 = 0.54 \pm 0.15, p \leq 0.001$). Indeed, the W/W_0-values measured for OA and OB were found to be significantly different ($p \leq 0.001$), indicating that both oligomers reduce cell-substrate interaction, yet with different efficiencies.

To better describe the role of GM1, particularly of its sialic acid moiety, in cell-oligomer interaction, the same experiments were repeated with NAA-treated cells. In this case, adhesion to PDL of sialic-acid-lacking cells was affected similarly after OA or OB administration ($p > 0.05$); in particular, W/W_0-values of 0.55 ± 0.13 and of 0.63 ± 0.13 were recorded in the presence of OA or OB, respectively (Fig. 3 *B*). These data suggest that OAs, but not OBs, interact with the cell membrane largely through GM1 sites, in addition to membrane proteins (unpublished data), and that the sialic acid component of GM1 is involved in such interaction. The raw data (nonnormalized) were shown in the Supporting Material.

RGD administration affects the affinity between OA/OB and the cell membrane

The RGD sequence found in many extracellular matrix components (such as fibronectin, laminin, and vitronectin) plays a fundamental role in cell adhesion through the interaction with a large class of integrin receptors (65). In a recent paper, we reported the prominent role of RGD-binding integrins in the first step of cell adhesion (52). Therefore, to match those results with the data reported above, we investigated the importance of the RGD sequence for OA and OB binding to the cells by using multifunctional substrates containing PDL. F-D curves were acquired with single NAA-treated or NAA-untreated CHO cells before and after the addition of a solution containing the RGD sequence (Fig. 4 *A*), as described in Materials and Methods. Over 15 F-D curves for each spot were acquired for every single cell. Twelve untreated and 12 NAA-treated CHO cells were tested, allowing the recording of 203 and 198 F-D curves, respectively. After RGD administration, a total number of 187 and 192 F-D curves were acquired on untreated or NAA-treated cells, respectively.

We found that cell adhesion to PDL was higher than cell adhesion to OA or OB (Fig. S3). NAA treatment did not significantly affect the interaction of CHO cells with PDL or OB, implying the lack of participation of GM1 in such interaction; however, NAA treatment significantly reduced cell interaction with OA (Fig. S3), confirming the experiments shown in Fig. 2 *B* and the importance of GM1. The addition of the RGD sequence dramatically decreased cell adhesion at each experimental condition, yet with different levels of effectiveness (Fig. 4, *B–G*). Also, in this case the *W* data were normalized to the *W*-value obtained in the absence of RGD, i.e., W_0. As expected, the detachment work from PDL was strongly reduced after RGD administration in NAA-untreated cells ($W/W_0 = 0.11 \pm 0.06$), in agreement with previous results (52). However, a significant, yet less evident, decrease after RGD addition was also observed with OA ($W/W_0 = 0.31 \pm 0.06$) and OB ($W/W_0 = 0.52 \pm 0.07$).

In NAA-treated CHO cells, the observed values of W/W_0 on PDL and OB after RGD injection underwent a similar decrease, within experimental error, to those obtained with NAA-untreated cells ($W/W_0 = 0.16 \pm 0.01$ and $W/W_0 = 0.59 \pm 0.04$, respectively), implying that, although involved in cell adhesion (66–69), GM1 does not play a prominent role in PDL-cell interaction and is not involved in the binding between cells and OB. However, a reduced decrease of the W/W_0-value on OA was observed after RGD administration, showing the same behavior as OB ($W/W_0 = 0.56 \pm 0.06$). This suggests that RGD only in part hinders cell binding to OA via GM1 and that RGD binding to cell membrane proteins does not directly involve membrane gangliosides.

The reduced capability of OA and OB to bind to the cell membrane after RGD administration has been demonstrated by using an alternative technique, i.e., confocal fluorescence microscopy on immunostained samples on untreated and NAA-treated CHO cells (Fig. S4), corroborating the findings obtained by AFM. From all these data, we conclude that both HypF-N oligomers affect cell adhesion capability,

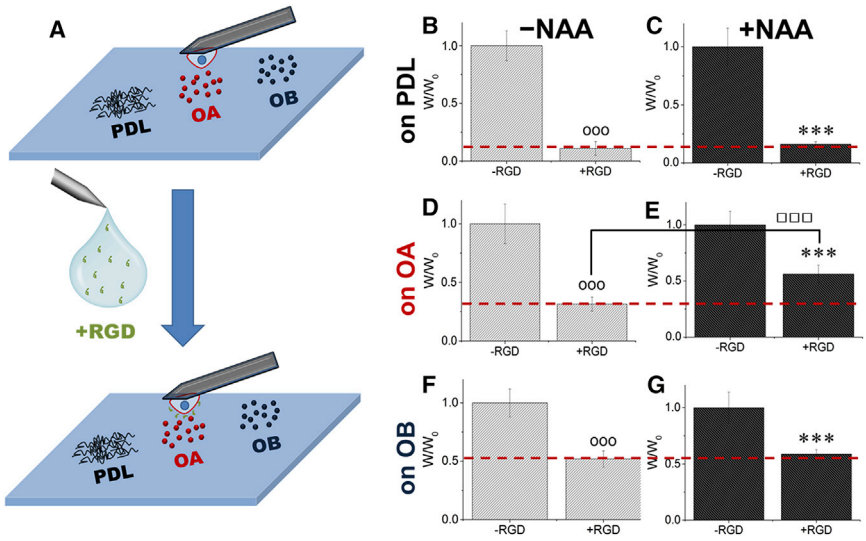

FIGURE 4 (*A*) shows a schematic representation of the distribution of molecules on the glass substrate. A first set of F-D curves was acquired on the molecular spots (OA, OB, and PDL) in both NAA-untreated and NAA-treated CHO cells; then RGD was added at a final concentration of 200 μM and incubated for 25 min before the acquisition of a new set of F-D curves. (*B*)–(*G*) show the mean work spent to detach the cell from PDL (*B*) and (*C*), OA (*D*) and (*E*), and OB (*F*) and (*G*) in NAA-untreated ((*B*), (*D*), and (*F*)) and NAA-treated ((*C*), (*E*), and (*G*)) cells, and before (*left bars*) and after (*right bars*) RGD addition. All *W*-values were normalized to the corresponding values obtained in the absence of RGD (W_0). Error bars correspond to standard deviations. *** and $^{\circ\circ\circ}$ indicate $p \leq 0.001$ relative to the corresponding values in the absence of RGD. $^{\square\square\square}$ indicates $p \leq 0.001$ in the indicated comparison. To see this figure in color, go online.

yet with different efficiencies, but only in the case of OA is this effect largely mediated by GM1, thus providing further clues suggesting preferential oligomer interaction with membrane lipids rather than proteins.

OA affects CHO cell adhesion and proliferation

Finally, taking into consideration the close relationship between cell adhesion and proliferation, we investigated the ability of CHO cells to adhere and proliferate on PDL-coated substrates in the absence or presence of 12 μM OA or OB (monomer equivalents). Confocal microscopy images were acquired 24 and 48 h after cell seeding, and the results were compared with those obtained with control experiments carried out in the absence of HypF-N oligomers (Fig. 5). In the absence of HypF-N oligomers, the cells were found to be healthy and spreading already at 24 h after seeding (Fig. 5 *A*), with increased cell number and spreading at 48 h (Fig. 5 *E*). Similar results were found with cells exposed to OB (Fig. 5, *B* and *F*). Considering that the effects of OB were similar in NAA-treated and NAA-untreated cells in previous experiments, these experiments were not repeated with NAA-treated cells (Fig. 5). By contrast, after 24 h exposure, a large number of OA-exposed cells showed a spherical shape, a morphology associated with detached or weakly adherent cells (Fig. 5 *C*). This phenotype changed further after 48 h, when the cells tended to cluster, forming large clumps of spherical cells (Figs. 5 *G* and 6). A normal phenotype was found in OA-exposed cells seeded after treatment with NAA; in this case, cell number and spreading were not perturbed, and cell behavior was similar to that found in cells cultured in the absence of HypF-N oligomers (Figs. 5, *D* and *H* and 6). High-resolution images of all samples fixed at 48 h are also shown (Fig. 5, *I*–*L*). The level of cell spreading after 48 h was quantified (Fig. 6).

Taken together, these data confirm those reported above on the interference of HypF-N oligomers, notably OA, with cell adhesion to the substrate, a function needed for cell proliferation that appears to be unaffected in NAA-treated cells. These data also suggest that cell proliferation and migration are likely to be affected by oligomer binding to GM1, which involves its sialic acid moiety.

DISCUSSION

It is increasingly recognized that the interaction of protein-misfolded oligomers with the cell membrane is an early event in the sequence of biochemical modifications that eventually culminate with cell impairment and death. Recent research has highlighted the importance of both oligomer structure/morphology and membrane physicochemical features as key determinants of oligomer cytotoxicity, mainly arising from different timing/conditions of oligomer growth and different lipid content, respectively (13,14,18,70,71). In this context, lipid rafts have emerged as pivotal players of oligomer recruitment and cytotoxicity (18,72,73). Therefore, it is important to use new methods to describe in detail and accurately measure the affinities of different types of protein aggregates to cell membranes containing different lipid contents.

Our study provided clues on these issues by exploiting a novel, to our knowledge, approach to investigate the interactions and measure the strength of the intermolecular bonds established between two types of HypF-N oligomers with similar morphological properties yet different cytotoxicity and the cell membrane. To do this, we determined the interaction strength between the cell membrane of CHO cells and both toxic and nontoxic oligomers of the sample protein HypF-N by calculating the work spent to detach the cell from the oligomers. We found that the

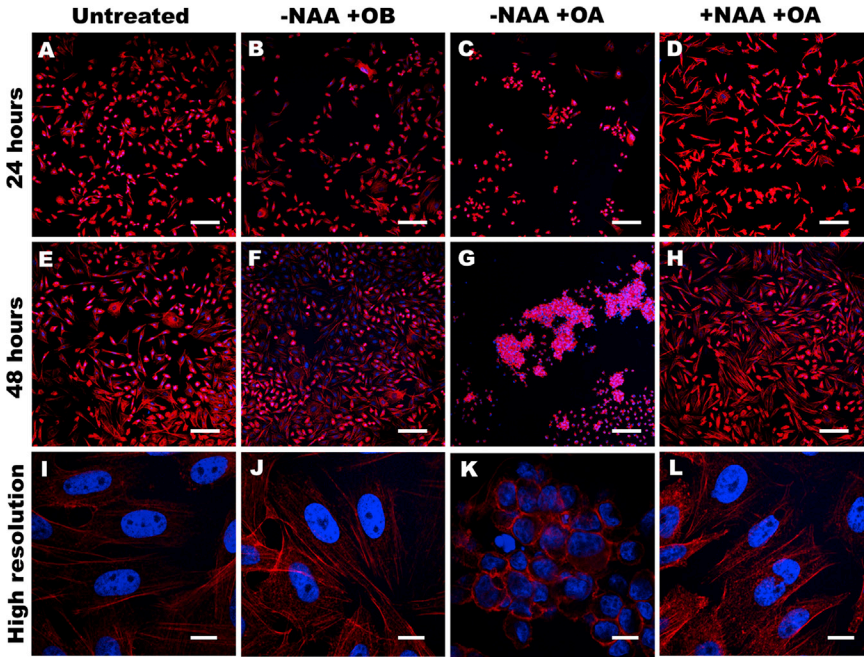

FIGURE 5 Confocal microscopy images of CHO cells 24 h (*A–D*) and 48 h (*E–L*) after seeding on PDL-coated substrates in the absence of HypF-N oligomers ((*A*), (*E*), and (*I*)), in the presence of OB ((*B*), (*F*), and (*J*)), in the presence of OA ((*C*), (*G*), and (*K*)), and in NAA-treated cells in the presence of OA ((*D*), (*H*), and (*L*)). In all panels the blue fluorescence, produced by 4′, 6-diamidino-2-phenylindole, shows the cell nuclei, whereas the red fluorescence, produced by Alexa Fluor-647 phalloidin, shows F-actin. Scale bars: 200 μm (*A–H*) and 10 μm (*I–L*). To see this figure in color, go online.

strength of the toxic oligomers of HypF-N was approximately twice as large as that of the nontoxic species of the same protein.

We were also able to determine the contribution of membrane proteins and membrane lipids to the binding affinity of the toxic species for the cell membrane in terms of detachment work. This results from the following analysis. Removal of the sialic group of the GM1 ganglioside, which is the main mediator of the lipid-oligomer interaction and associated toxicity, reduces to approximately one-half of the affinity of the toxic oligomers for the membrane. Since it was previously found that removal of the GM1 sialic acid group from SLBs cancels out toxic OA binding to the GM1-containing gel phase domains while maintaining that to the fluid phase domains (18), the residual affinity observed between the toxic oligomers and the GM1-deprived cells is likely to result from oligomer binding to the disordered fluid phase of the membrane (non-lipid rafts) and to the protein components of the membrane. Indeed, both toxic and nontoxic HypF-N oligomers were able to bind to membrane proteins, with the nontoxic species displaying a slightly higher affinity (Mannini et al., in preparation), and only toxic oligomers were able to bind to the liquid phase of the membrane (18), suggesting why the affinities of toxic and nontoxic species for the GM1-deprived cells are similar for the two species. It can therefore be concluded that the GM1-containing lipid rafts contribute to approximately one-half of the overall affinity between the toxic oligomers and the cell membrane, and that the remaining half is contributed by the proteins and non-lipid-raft phospholipids. This is an interesting outcome, considering the unresolved question as to whether aggregate interaction with the cell membrane involves specific or generic lipids of the bilayer, specific or generic membrane proteins, or both, and, in the case of membrane proteins, whether such interaction is direct or mediated by surrounding lipids.

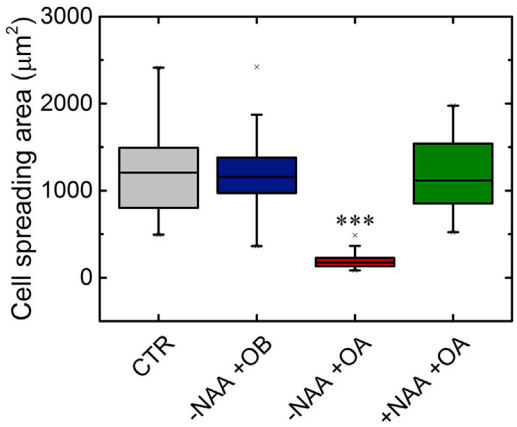

FIGURE 6 The area occupied on the substrate by single CHO cells seeded in the presence of OB (−NAA+OB) is compatible with the area measured in the CTR. Cell spreading is significantly reduced ($p < 0.001$) for CHO cells seeded in the presence of toxic OA (−NAA+OA). Cell adhesion capability in the presence of OA is recovered in NAA treated cells (+NAA+OA). To see this figure in color, go online.

We also studied, for the first time as far as we know, the effects of two types of toxic and nontoxic oligomers on cell adhesion, proliferation, and spreading, providing information that adds another piece to the oligomer toxicity jigsaw puzzle. At the present, there is an increasing knowledge of the biophysical, biochemical, and molecular features of oligomer interaction with exposed cells either at lipid or at

protein membrane components; however, so far very few data have been reported about the possible role played by a third important element of the system, i.e., the extracellular matrix and its protein content, in modulating the interference of amyloid oligomers with cell viability and physiology. Yet the extracellular matrix plays pivotal roles in cell adhesion, mobility, proliferation, and differentiation, favoring cell viability and correct responses to environmental physiological or pathological stimuli, including those arising from the presence of amyloid oligomers (74,75). More knowledge on this aspect appears of importance to get a more complete description of the molecular basis of oligomer-mediated cell modifications underlying cytotoxicity. Our data demonstrate that after RGD administration, the mechanical work decreases, reaching roughly the same value in all the conditions (PDL, OA, and OB, with and without NAA), as shown in Fig. S3, *C* and *D*. RGD injection not only blocks the integrins, but also influences ganglioside functionality. Indeed, it has been repeatedly reported that gangliosides play a role in cell adhesion by binding fibronectin at its binding site, i.e., the RGD domain (66–69). For this reason, the RGD injection has a double effect: it blocks the direct binding of integrins to OA (a minor fraction for OA) and it blocks/disturbs OA binding to GM1. As a consequence, the *W*-value after RGD administration is the same in the different conditions, because in all conditions the same interactions, i.e., the binding of PDL, OA, and OB to integrins and to the gangliosides, have been blocked. However, only in the case of OA is a large part of the interaction hindered by the removal of the sialic acid moiety from GM1 before RGD administration. This confirmed the high affinity of OA and only OA for GM1. Overall, the data reported here suggest that the toxic oligomers characterized by a higher affinity to the cell membrane, particularly at GM1 sites, in addition to the GM1 functionality, could affect the activity of a large class of RGD-binding proteins. These two events contribute together to influence some features of cell adhesion and the ensuing modifications, including cell mobility and spreading. In particular, we found that oligomer, notably OA, binding to the cells hindered both proliferation and spreading, and also in this case the presence of the sialic acid component of GM1 appeared to drive the observed modifications.

All these effects are likely to contribute to the toxicity of OA to cells both in culture and in tissue. The results presented here provide, to our knowledge, new and valuable hints on the mechanism of interaction between amyloid aggregates and cellular membrane, although it must be considered that the physiological target in neural diseases are brain cells. These data also agree with previous results on single-molecule tracking that showed a modification of GM1 mobility on the membrane of SH-SY5Y cells upon interaction with a type of $A\beta_{42}$ oligomers, named A+, with structural and biological properties comparable to those of OA in terms of solvent-exposed hydrophobicity and toxicity, whereas no modifications were observed in the presence of the other type of Aβ oligomers, named A−, comparable to OB for the same structural and biological characteristics (25).

CONCLUSIONS

We applied for the first time, to our knowledge, an AFM-based single-cell technique to the study of the interaction between misfolded protein oligomers and the cell membrane. In particular, by measuring the mechanical work (*W*) spent to completely detach the oligomers from the cell, we showed that toxic and nontoxic oligomers grown from HypF-N bind to the cell membrane with different efficiency. The oligomer-cell membrane interaction strength appears to be a key determinant of oligomer cytotoxicity and is mediated by the presence of the negatively charged sialic acid group of the ganglioside GM1, in agreement with previously reported data on cytotoxicity. We were also able to discriminate the contributions provided by membrane lipids and membrane proteins to oligomer-cell binding. Finally, we showed that the presence of toxic OA significantly alters cell adhesion capability. In particular, we observed that the interaction of toxic OA with the cell membrane significantly affects the functionality of a class of adhesion molecules, RGD binding proteins, and that this effect requires the presence of GM1, particularly of its negatively charged sialic acid moiety.

SUPPORTING MATERIAL

Four figures are available at http://www.biophysj.org/biophysj/supplemental/S0006-3495(18)30202-9.

AUTHOR CONTRIBUTIONS

R.O.-N. designed and performed research, analyzed data, and wrote the manuscript. S.K. helped in performing research. S.D. designed research and wrote the manuscript. A.D. designed research and wrote the manuscript. B.M. helped with designing research. C. Capitini helped with performing research. C. Cecchi designed research. M.S. designed research and wrote the manuscript. F.C. designed research and wrote the manuscript. C. Canale designed research, analyzed data, and wrote the manuscript.

REFERENCES

1. Chiti, F., and C. M. Dobson. 2017. Protein misfolding, amyloid formation, and human disease: a summary of progress over the last decade. *Annu. Rev. Biochem.* 86:27–68.

2. Cremades, N., S. I. Cohen, …, D. Klenerman. 2012. Direct observation of the interconversion of normal and toxic forms of α-synuclein. *Cell.* 149:1048–1059.

3. Lasagna-Reeves, C. A., C. G. Glabe, and R. Kayed. 2011. Amyloid-β annular protofibrils evade fibrillar fate in Alzheimer disease brain. *J. Biol. Chem.* 286:22122–22130.

4. Pires, R. H., M. J. Saraiva, …, M. S. Z. Kellermayer. 2011. Structure and assembly-disassembly properties of wild-type transthyretin amyloid protofibrils observed with atomic force microscopy. *J. Mol. Recognit.* 24:467–476.
5. Stroud, J. C., C. Liu, …, D. Eisenberg. 2012. Toxic fibrillar oligomers of amyloid-β have cross-β structure. *Proc. Natl. Acad. Sci. USA.* 109:7717–7722.
6. Martins, I. C., I. Kuperstein, …, F. Rousseau. 2008. Lipids revert inert Abeta amyloid fibrils to neurotoxic protofibrils that affect learning in mice. *EMBO J.* 27:224–233.
7. Lesné, S., M. T. Koh, …, K. H. Ashe. 2006. A specific amyloid-beta protein assembly in the brain impairs memory. *Nature.* 440:352–357.
8. Koffie, R. M., M. Meyer-Luehmann, …, T. L. Spires-Jones. 2009. Oligomeric amyloid β associates with postsynaptic densities and correlates with excitatory synapse loss near senile plaques. *Proc. Natl. Acad. Sci. USA.* 106:4012–4017.
9. Cohen, S. I. A., S. Linse, …, T. P. J. Knowles. 2013. Proliferation of amyloid-β42 aggregates occurs through a secondary nucleation mechanism. *Proc. Natl. Acad. Sci. USA.* 110:9758–9763.
10. Buell, A. K., C. Galvagnion, …, C. M. Dobson. 2014. Solution conditions determine the relative importance of nucleation and growth processes in α-synuclein aggregation. *Proc. Natl. Acad. Sci. USA.* 111:7671–7676.
11. Kakkar, V., C. Månsson, …, H. H. Kampinga. 2016. The S/T-rich motif in the DNAJB6 chaperone delays polyglutamine aggregation and the onset of disease in a mouse model. *Mol. Cell.* 62:272–283.
12. Meisl, G., X. Yang, …, T. P. Knowles. 2014. Differences in nucleation behavior underlie the contrasting aggregation kinetics of the Aβ40 and Aβ42 peptides. *Proc. Natl. Acad. Sci. USA.* 111:9384–9389.
13. Campioni, S., B. Mannini, …, F. Chiti. 2010. A causative link between the structure of aberrant protein oligomers and their toxicity. *Nat. Chem. Biol.* 6:140–147.
14. Evangelisti, E., C. Cecchi, …, M. Stefani. 2012. Membrane lipid composition and its physicochemical properties define cell vulnerability to aberrant protein oligomers. *J. Cell Sci.* 125:2416–2427.
15. Evangelisti, E., R. Cascella, …, C. Cecchi. 2016. Binding affinity of amyloid oligomers to cellular membranes is a generic indicator of cellular dysfunction in protein misfolding diseases. *Sci. Rep.* 6:32721.
16. Mannini, B., R. Cascella, …, F. Chiti. 2012. Molecular mechanisms used by chaperones to reduce the toxicity of aberrant protein oligomers. *Proc. Natl. Acad. Sci. USA.* 109:12479–12484.
17. Mannini, B., E. Mulvihill, …, F. Chiti. 2014. Toxicity of protein oligomers is rationalized by a function combining size and surface hydrophobicity. *ACS Chem. Biol.* 9:2309–2317.
18. Oropesa-Nuñez, R., S. Seghezza, …, C. Canale. 2016. Interaction of toxic and non-toxic HypF-N oligomers with lipid bilayers investigated at high resolution with atomic force microscopy. *Oncotarget.* 7:44991–45004.
19. Tatini, F., A. M. Pugliese, …, F. Chiti. 2013. Amyloid-β oligomer synaptotoxicity is mimicked by oligomers of the model protein HypF-N. *Neurobiol. Aging.* 34:2100–2109.
20. Zampagni, M., R. Cascella, …, C. Cecchi. 2011. A comparison of the biochemical modifications caused by toxic and non-toxic protein oligomers in cells. *J. Cell. Mol. Med.* 15:2106–2116.
21. Stefani, M. 2012. Structural features and cytotoxicity of amyloid oligomers: implications in Alzheimer's disease and other diseases with amyloid deposits. *Prog. Neurobiol.* 99:226–245.
22. Cecchi, C., and M. Stefani. 2013. The amyloid-cell membrane system. The interplay between the biophysical features of oligomers/fibrils and cell membrane defines amyloid toxicity. *Biophys. Chem.* 182:30–43.
23. Ladiwala, A. R., J. Litt, …, P. M. Tessier. 2012. Conformational differences between two amyloid β oligomers of similar size and dissimilar toxicity. *J. Biol. Chem.* 287:24765–24773.
24. Calamai, M., and F. S. Pavone. 2013. Partitioning and confinement of GM1 ganglioside induced by amyloid aggregates. *FEBS Lett.* 587:1385–1391.
25. Calamai, M., E. Evangelisti, …, F. Pavone. 2016. Single molecule experiments emphasize GM1 as a key player of the different cytotoxicity of structurally distinct Aβ1–42 oligomers. *Biochim. Biophys. Acta.* 1858:386–392.
26. Calamai, M., and F. S. Pavone. 2011. Single molecule tracking analysis reveals that the surface mobility of amyloid oligomers is driven by their conformational structure. *J. Am. Chem. Soc.* 133:12001–12008.
27. Wakabayashi, M., and K. Matsuzaki. 2009. Ganglioside-induced amyloid formation by human islet amyloid polypeptide in lipid rafts. *FEBS Lett.* 583:2854–2858.
28. Fantini, J., N. Yahi, and N. Garmy. 2013. Cholesterol accelerates the binding of Alzheimer's β-amyloid peptide to ganglioside GM1 through a universal hydrogen-bond-dependent sterol tuning of glycolipid conformation. *Front. Physiol.* 4:120.
29. Ikeda, K., T. Yamaguchi, …, K. Matsuzaki. 2011. Mechanism of amyloid β-protein aggregation mediated by GM1 ganglioside clusters. *Biochemistry.* 50:6433–6440.
30. Hong, S., B. L. Ostaszewski, …, D. J. Selkoe. 2014. Soluble Aβ oligomers are rapidly sequestered from brain ISF in vivo and bind GM1 ganglioside on cellular membranes. *Neuron.* 82:308–319.
31. Cebecauer, M., M. Hof, and M. Amaro. 2017. Impact of GM1 on membrane-mediated aggregation/oligomerization of β-amyloid: unifying view. *Biophys. J.* 113:1194–1199.
32. Calamai, M., N. Taddei, …, F. Chiti. 2003. Relative influence of hydrophobicity and net charge in the aggregation of two homologous proteins. *Biochemistry.* 42:15078–15083.
33. Kayed, R., A. Pensalfini, …, C. Glabe. 2009. Annular protofibrils are a structurally and functionally distinct type of amyloid oligomer. *J. Biol. Chem.* 284:4230–4237.
34. Kayed, R., Y. Sokolov, …, C. G. Glabe. 2004. Permeabilization of lipid bilayers is a common conformation-dependent activity of soluble amyloid oligomers in protein misfolding diseases. *J. Biol. Chem.* 279:46363–46366.
35. Stöckl, M. T., N. Zijlstra, and V. Subramaniam. 2013. α-Synuclein oligomers: an amyloid pore? Insights into mechanisms of α-synuclein oligomer-lipid interactions. *Mol. Neurobiol.* 47:613–621.
36. van Rooijen, B. D., M. M. Claessens, and V. Subramaniam. 2010. Membrane permeabilization by oligomeric α-synuclein: in search of the mechanism. *PLoS One.* 5:e14292.
37. Jarosz-Griffiths, H. H., E. Noble, …, N. M. Hooper. 2016. Amyloid-β receptors: the good, the bad, and the prion protein. *J. Biol. Chem.* 291:3174–3183.
38. Horton, M., G. Charras, and P. Lehenkari. 2002. Analysis of ligand-receptor interactions in cells by atomic force microscopy. *J. Recept. Signal Transduct. Res.* 22:169–190.
39. Eibl, R. H., and V. T. Moy. 2005. Atomic force microscopy measurements of protein-ligand interactions on living cells. *In* Protein-Ligand Interactions: Methods and Applications. G. U. Nienhaus, ed. Humana Press, pp. 439–449.
40. Pfreundschuh, M., D. Alsteens, …, D. J. Müller. 2015. Identifying and quantifying two ligand-binding sites while imaging native human membrane receptors by AFM. *Nat. Commun.* 6:8857.
41. Chen, A., and V. T. Moy. 2000. Cross-linking of cell surface receptors enhances cooperativity of molecular adhesion. *Biophys. J.* 78:2814–2820.
42. Zhang, X., E. Wojcikiewicz, and V. T. Moy. 2002. Force spectroscopy of the leukocyte function-associated antigen-1/intercellular adhesion molecule-1 interaction. *Biophys. J.* 83:2270–2279.
43. Christenson, W. B. 2016. Binding forces of single αMβ2 integrin-fibrinogen interactions on living cells. *Biophys. J.* 110:620a.
44. Chtcheglova, L. A., J. Waschke, …, P. Hinterdorfer. 2007. Nano-scale dynamic recognition imaging on vascular endothelial cells. *Biophys. J.* 93:L11–L13.
45. Shaw, J. E., R. F. Epand, …, C. M. Yip. 2006. Correlated fluorescence-atomic force microscopy of membrane domains: structure of fluorescence probes determines lipid localization. *Biophys. J.* 90:2170–2178.

46. Rotsch, C., and M. Radmacher. 2000. Drug-induced changes of cytoskeletal structure and mechanics in fibroblasts: an atomic force microscopy study. *Biophys. J.* 78:520–535.

47. Müller, D. J., and Y. F. Dufrêne. 2008. Atomic force microscopy as a multifunctional molecular toolbox in nanobiotechnology. *Nat. Nanotechnol.* 3:261–269.

48. Franz, C. M., and P.-H. Puech. 2008. Atomic force microscopy: a versatile tool for studying cell morphology, adhesion and mechanics. *Cell. Mol. Bioeng.* 1:289–300.

49. Franz, C. M., A. Taubenberger, …, D. J. Muller. 2007. Studying integrin-mediated cell adhesion at the single-molecule level using AFM force spectroscopy. *Sci. STKE.* 2007:pl5.

50. Friedrichs, J., J. Helenius, and D. J. Muller. 2010. Quantifying cellular adhesion to extracellular matrix components by single-cell force spectroscopy. *Nat. Protoc.* 5:1353–1361.

51. Benoit, M., D. Gabriel, …, H. E. Gaub. 2000. Discrete interactions in cell adhesion measured by single-molecule force spectroscopy. *Nat. Cell Biol.* 2:313–317.

52. Canale, C., A. Petrelli, …, S. Dante. 2013. A new quantitative experimental approach to investigate single cell adhesion on multifunctional substrates. *Biosens. Bioelectron.* 48:172–179.

53. Helenius, J., C.-P. Heisenberg, …, D. J. Muller. 2008. Single-cell force spectroscopy. *J. Cell Sci.* 121:1785–1791.

54. Taubenberger, A., D. A. Cisneros, …, C. M. Franz. 2007. Revealing early steps of α2β1 integrin-mediated adhesion to collagen type I by using single-cell force spectroscopy. *Mol. Biol. Cell.* 18:1634–1644.

55. Panorchan, P., M. S. Thompson, …, D. Wirtz. 2006. Single-molecule analysis of cadherin-mediated cell-cell adhesion. *J. Cell Sci.* 119:66–74.

56. Saridaki, T., M. Zampagni, …, F. Chiti. 2012. Glycosaminoglycans (GAGs) suppress the toxicity of HypF-N prefibrillar aggregates. *J. Mol. Biol.* 421:616–630.

57. Kuwabara, K., K. Nishitsuji, …, N. Sakashita. 2015. Cellular interaction and cytotoxicity of the iowa mutation of apolipoprotein A-I (ApoA-IIowa) amyloid mediated by sulfate moieties of heparan sulfate. *J. Biol. Chem.* 290:24210–24221.

58. Chang, K. L., H. N. Pee, …, P. C. Ho. 2015. Metabolic profiling of CHO-AβPP695 cells revealed mitochondrial dysfunction prior to amyloid-β pathology and potential therapeutic effects of both PPARγ and PPARα Agonisms for Alzheimer's disease. *J. Alzheimers Dis.* 44:215–231.

59. Puech, P.-H., A. Taubenberger, …, C.-P. Heisenberg. 2005. Measuring cell adhesion forces of primary gastrulating cells from zebrafish using atomic force microscopy. *J. Cell Sci.* 118:4199–4206.

60. Hutter, J. L., and J. Bechhoefer. 1993. Calibration of atomic-force microscope tips. *Rev. Sci. Instrum.* 64:1868–1873.

61. Ferrera, D., C. Canale, …, L. Gasparini. 2014. Lamin B1 overexpression increases nuclear rigidity in autosomal dominant leukodystrophy fibroblasts. *FASEB J.* 28:3906–3918.

62. Azeloglu, E. U., and K. D. Costa. 2011. Atomic force microscopy in mechanobiology: measuring microelastic heterogeneity of living cells. *In* Atomic Force Microscopy in Biomedical Research: Methods and Protocols. P. C. Braga and D. Ricci, eds. Humana Press, pp. 303–329.

63. Bucciantini, M., E. Giannoni, …, M. Stefani. 2002. Inherent toxicity of aggregates implies a common mechanism for protein misfolding diseases. *Nature.* 416:507–511.

64. Bucciantini, M., G. Calloni, …, M. Stefani. 2004. Prefibrillar amyloid protein aggregates share common features of cytotoxicity. *J. Biol. Chem.* 279:31374–31382.

65. Pierschbacher, M. D., and E. Ruoslahti. 1984. Variants of the cell recognition site of fibronectin that retain attachment-promoting activity. *Proc. Natl. Acad. Sci. USA.* 81:5985–5988.

66. Kleinman, H. K., G. R. Martin, and P. H. Fishman. 1979. Ganglioside inhibition of fibronectin-mediated cell adhesion to collagen. *Proc. Natl. Acad. Sci. USA.* 76:3367–3371.

67. Pytela, R., M. D. Pierschbacher, and E. Ruoslahti. 1985. Identification and isolation of a 140 kd cell surface glycoprotein with properties expected of a fibronectin receptor. *Cell.* 40:191–198.

68. Perkins, R. M., S. Kellie, …, D. R. Critchley. 1982. Gangliosides as receptors for fibronectin? Comparison of cell spreading on a ganglioside-specific ligand with that on fibronectin. *Exp. Cell Res.* 141:231–243.

69. Yamada, K. M., D. R. Critchley, …, J. Moss. 1983. Exogenous gangliosides enhance the interaction of fibronectin with ganglioside-deficient cells. *Exp. Cell Res.* 143:295–302.

70. Krishnan, R., J. L. Goodman, …, S. Lindquist. 2012. Conserved features of intermediates in amyloid assembly determine their benign or toxic states. *Proc. Natl. Acad. Sci. USA.* 109:11172–11177.

71. Valincius, G., F. Heinrich, …, M. Lösche. 2008. Soluble amyloid β-oligomers affect dielectric membrane properties by bilayer insertion and domain formation: implications for cell toxicity. *Biophys. J.* 95:4845–4861.

72. Cecchi, C., D. Nichino, …, A. Relini. 2009. A protective role for lipid raft cholesterol against amyloid-induced membrane damage in human neuroblastoma cells. *Biochim. Biophys. Acta.* 1788:2204–2216.

73. Cascella, R., E. Evangelisti, …, C. Cecchi. 2017. Soluble oligomers require a ganglioside to trigger neuronal calcium overload. *J. Alzheimers Dis.* 60:923–938.

74. Marastoni, S., G. Ligresti, …, M. Mongiat. 2008. Extracellular matrix: a matter of life and death. *Connect. Tissue Res.* 49:203–206.

75. Lau, L. W., R. Cua, …, V. W. Yong. 2013. Pathophysiology of the brain extracellular matrix: a new target for remyelination. *Nat. Rev. Neurosci.* 14:722–729.